Optical Materials 35 (2013) 1636–1641

Contents lists available at SciVerse ScienceDirect

Optical Materials

journal homepage: www.elsevier.com/locate/optmat

# Optical properties and Judd–Ofelt parameters of $Dy^{3+}$ doped $K_2GdF_5$ single crystal

Phan Van Do [a], Vu Phi Tuyen [b], Vu Xuan Quang [c], Nguyen Trong Thanh [b], Vu Thi Thai Ha [b], Ho Van Tuyen [c], Nicholas M. Khaidukov [d], Julián Marcazzó [e], Yong-Ill Lee [f], Bui The Huy [f,*]

[a] Water Resources University, 175 Tay Son Street, Hanoi, Viet Nam
[b] Institute of Materials Science, Vietnam Academy of Science and Technology, 18 Hoang Quoc Viet Street, Hanoi, Viet Nam
[c] Duy Tan University, K7/25 Quang Trung, DaNang, Viet Nam
[d] Kurnakov Institute of General and Inorganic Chemistry, Moscow, Russia
[e] IFAS, Facultad de Ciencias Exactas, Universidad Nacional del Centro de la Provincia de Buenos Aires, Pinto 399, 7000 Tandil, Argentina
[f] Department of Chemistry, Changwon National University, Changwon 641 773, South Korea

ARTICLE INFO

*Article history:*
Received 20 February 2013
Received in revised form 27 March 2013
Accepted 12 April 2013
Available online 18 May 2013

*Keywords:*
Judd–Ofelt
Rare earth alloys and compounds
Optical properties
Crystal and ligand fields

ABSTRACT

$Dy^{3+}$-doped $K_2GdF_5$ single crystals with 10.0 mol% have been prepared by hydrothermal condition. The spectra are analyzed in term of the Judd–Ofelt theory, the intensity parameters ($\Omega_\lambda$, $\lambda = 2, 4, 6$) have been evaluated for $Dy^{3+}$-doped $K_2GdF_5$ sample. The electric ($S_{ed}$), magnetic ($S_{md}$) dipole line strength, radiative ($A$), and total radiative ($A_T$) transition probabilities, lifetime ($\tau_R$), branching ratios ($\beta_R$) for the excited levels of $Dy^{3+}$ doped $K_2GdF_5$ crystals were investigated by using the intensity parameters. In addition, the stimulated emission cross-sections ($\sigma_{\lambda p}$) and integrated emission cross-section ($\Sigma_{if}$) have been predicted for the transitions from excited level, $^4F_{9/2}$, to the $^6H_{15/2}$, $^6H_{13/2}$ and $^6H_{11/2}$ levels. The energy transfer occurs from $Gd^{3+}$ to $Dy^{3+}$, resulting in the additional intense excitation UV-narrow bands for the luminescence of the $Dy^{3+}$ ions.



## 1. Introduction

Rare-earth elements are of interest in several high-tech and environmental application areas. Glasses have been known as a convenient host for rare earths and have been widely used. The rare earths (RE) doped glasses provide basically scientific information, such as energy level structure, radiative properties, stimulated emission cross-sections, etc. These information help to develop new optical materials and improve the existing devices like lasers, light converters, sensors, high density memories, and optical fibers and amplifiers [1–5].

In recent years, one of the most interesting fields of research is focused on the development of optical devices based on RE ions doped AF-A′F-$LnF_3$ systems (A, A′-alkali element, Ln-rare earth (RE) element), such as $K_2YF_5$ and $K_2GdF_5$ crystals. They are the materials of great promise for applications in optical area such as optical amplifiers, solid-state lasers [6] and especially they are a high energy dosimeter materials for great promise [7,8]. There have been many reports on spectrum properties of these materials such as the $K_2YF_5$:$Nd^{3+}$, $K_2YF_5$:$Tb^{3+}$, $K_2YF_5$:$Tm^{3+}$, $K_2YF_5$:$Sm^{3+}$ crystals [6–13]. The authors have investigated the optical properties of these materials by using optically stimulated luminescence (OSL) [10], thermoluminescence [11], frequency up-conversion fluorescence [12], site-selective laser-excitation spectroscopy [13]. It is know that $Dy^{3+}$ is one of the most abundant rare earth elements, which is used also extensively in optical devices. Most studies are limited its spectra in various matrices [14–18] but $Dy^{3+}$ doped in $K_2LnF_5$ crystal have received relatively less attention than the other lanthanide ions despite many features of interest.

In the work presented here we have investigated the optical properties of $Dy^{3+}$ doped $K_2GdF_5$ crystal and the energy transfer from $Gd^{3+}$ to $Dy^{3+}$ ions. On the other hand, we have also used the Judd–Ofelt (JO) theory to determine intensity parameters $\Omega_\lambda$ ($\lambda = 2, 4, 6$) by analyzing the absorption spectrum of $K_2GdF_5$:$Dy^{3+}$ crystal, and calculated the radiative transition probabilities, branching ratios, radiative lifetimes of $^4H_{15/2}$ excited state, stimulated emission cross-section for selected and briefly discussed the application potential of $K_2GdF_5$:$Dy^{3+}$ on the efficient laser, white fluorescence lamp.

## 2. Experiments

The $K_2GdF_5$ crystals doped with 10 mol% of $Dy^{3+}$ ions were obtained by hydrothermal synthesis at the Kurnakov Institute of General and Inorganic Chemistry, Moscow, Russia [8]. In a typical experiment, $K_2GdF_5$:$Dy^{3+}$single crystal was grown from the mixture of Gd, $Dy_2O_3$ and KF at a temperature of 750 K, a pressure of 100–150 MPa. The temperature gradient along the reactor body was 3 K $cm^{-1}$. A proper choice of reaction conditions have allowed

* Corresponding author. Tel.: +82 55 213 3436; fax: +82 55 213 3439.
*E-mail address:* buithehuy.nt@gmail.com (B.T. Huy).

0925-3467/$ - see front matter © 2013 Elsevier B.V. All rights reserved.
http://dx.doi.org/10.1016/j.optmat.2013.04.014

to obtain $K_2GdF_5$ single crystal. The XRD pattern of $K_2GdF_5$:$Dy^{3+}$ have shown that the fluoride $K_2GdF_5$ crystallizes in orthorhombic system, space group Pnma, $a = 10.814$ A°, $b = 6.623$ A°, $c = 7.389$ A°. The resulted $K_2GdF_5$:$Dy^{3+}$single crystals were polished for the optical measurements. The optical absorption spectrum was performed using Jascco V670 spectrometer by wavelength scanning from 300 nm to 2000 nm. The photoluminescence (PL) and excitation spectra were recorded by Fluorolog-3 spectrophotometer, model FL3-22, Horiba Jobin Yvon. For the measurement of fluorescent lifetime, a laser excitation was provided by the third harmonic of 355 nm of a pulsed Nd:YAG laser, model GCR-230, Spectra Physics. Pulse duration and energy were approximately 5 ns and 0.35 J, respectively. The emission from the sample was collected by quartz lens and detected into optical system for fluorescent lifetime measurement. The R928 photomultiplier, Hamamatsu and MSO2000 oscilloscope, Tektronix were used for this measurement. The PMT signal was averaged on a digital oscilloscope and processed with a computer. All the measurements were performed at room temperature.

## 3. Judd–Ofelt theoretical background

The Judd–Ofelt (JO) theory was shown to be useful to characterize radiative transitions for RE-doped solids and to estimate the intensities of the transitions for rare-earth ions [9,15–18]. This theory defines a set of three intensity parameters, $\Omega_\lambda$ ($\lambda = 2, 4, 6$), that are sensitive to the environment of the rare-earth ions. The JO parameters are used to predict the radiative properties of excited states of $Ln^{3+}$ ion such as transition probabilities ($A_R$), radiative lifetime ($\iota_R$), branching ratios ($\beta_R$), and stimulated emission cross-sections ($\sigma_{\lambda p}$). The details of this theory were shown in previous reports. The Judd–Ofelt analysis is an effective tool to study the compositional dependence of the spectroscopic parameters of the $Dy^{3+}$ ions and to design the desired phosphors.

According to the JO theory [19], the electric dipole oscillator strength of a transition from the ground state to an excited state is given by

$$f_{cal} = \frac{8\pi^2 mc\nu}{3h(2J+1)} \times \frac{(n^2+2)^2}{9n} \sum_{\lambda=2,4,6} \Omega_\lambda \langle \Psi J \| U^\lambda \| \Psi' J' \rangle^2 \quad (1)$$

where $n$ is the refractive index of the material, $J$ is the total angular momentum of the ground state, $\Omega_\lambda$ are the JO intensity parameters and $\|U^\lambda\|^2$ are the squared doubly reduced matrix of the unit tensor operator of the rank $\lambda = 2, 4, 6$ are calculated from intermediate coupling approximation for a transition $|\psi J\rangle \rightarrow |\psi' J'\rangle$.

The oscillator strengths, $f_{exp}$, of the absorption bands were determined experimentally using the following formula [20]

$$f_{exp} = 4.318 \times 10^{-9} \int \alpha(\nu) d\nu \quad (2)$$

where $\alpha$ is molar extinction coefficient at energy $\nu$ ($cm^{-1}$). The $\alpha(\nu)$ values can be calculated from absorbance $A$ by using Lambert-Beer's law

$$A = \alpha(\nu) cd \quad (3)$$

where $c$ is concentration [dim: $L^{-3}$; units: $moll^{-1}$], $d$ is the optical path length [dim: L; units: cm].

The oscillator strength of the various observed transitions are evaluated through Eqs. (1) and (2). A least squares fitting approach is then used for Eq. (2) to determine $\Omega_\lambda$ parameters which give the best fit between experimental and calculate oscillator strength.

## 4. Results and discussion

### 4.1. Absorption and emission spectra

Absorption spectra of $Dy^{3+}$-doped $K_2GdF_5$ crystal in two bands of wavelength 300–400 nm and 700–1400 nm were showed in Fig. 1. There are 12 observed absorption peaks at 310, 322, 346, 361, 380, 388 nm in ultra-violet band and 790, 880, 1057, 1089, 1255, 1301 nm in near-infrared band, which are attributed to transitions from $^6H_{15/2}$ ground state to $^4L_{19/2}$, $^6P_{3/2}$, $^6P_{7/2}$, $^6P_{5/2}$, $^4I_{13/2}$, $^4F_{7/2}$, $^6F_{5/2}$, $^6F_{7/2}$, $^6H_{7/2}$, $^6F_{9/2}$, $^6F_{11/2}$, $^6H_{9/2}$ higher excited states in order of increasing wavelength, respectively, of $Dy^{3+}$ ions. The energy of these absorption transitions of $Dy^{3+}$ion in $K_2GdF_5$ host are also compared with $Dy^{3+}$-diluted acid solution (aqua-ion) system [21] and shown in Table 1.

As shown in Fig. 2, which illustrates the emission spectrum using the 365 nm excitation wavelength of xenon lamp source, three emission bands at 485, 575 and 667 nm which are attributed to transitions from $^4F_{9/2}$ to $^6H_{15/2}$, $^6H_{13/2}$ and $^6H_{11/2}$ states, respectively, of $Dy^{3+}$ions. But among of them, the yellow (Y) band (575 nm) corresponds to the hypersensitive transition $^4F_{9/2} \rightarrow {}^6H_{13/2}$, and the blue (B) band (485 nm) corresponds to the $^4F_{9/2} \rightarrow {}^6H_{15/2}$ transition are the dominant bands in the emission spectrum. It is worth pointing out that, the intensity of the Y-band depends much more on the $\Omega_2$ and $\Omega_6$ intensity parameters than on the $\Omega_4$ one, because the values of the reduced matrix elements of rank 2 and rank 6 for this transition are 0.0512 and 0.0573, respectively, whereas that of rank 4 is only 0.0172. On the other hand, the intensity of the B-band depends practically only the

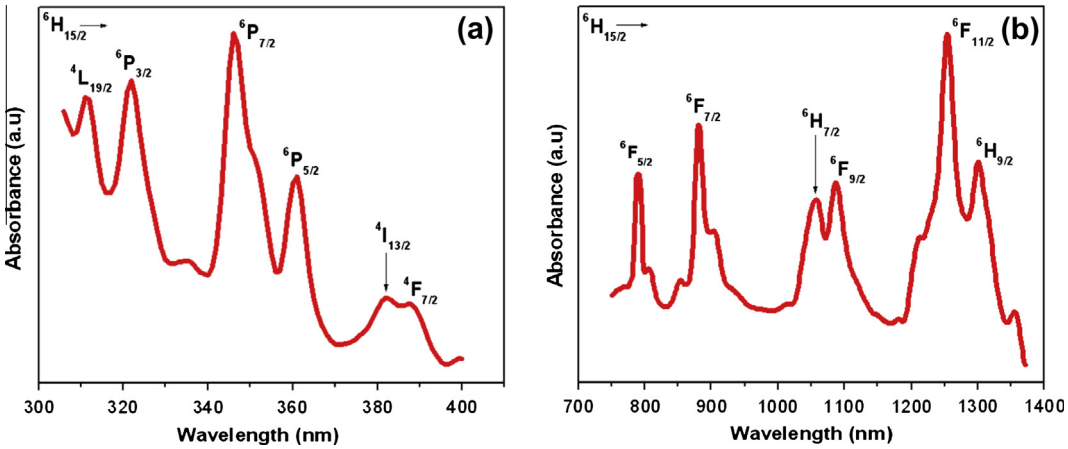


**Fig. 1.** The absorption spectra of $K_2GdF_5$:$Dy^{3+}$ crystal (a) in the range of ultra-violet light and (b) in the range of near infrared.

**Table 1**
Energy transitions ($v$), bonding parameters ($\delta$), the experimental ($f_{exp}$) and calculated ($f_{cal}$) oscillator strengths for $K_2GdF_5$:$Dy^{3+}$ crystal.

| Transition $^4H_{15/2}\rightarrow$ | $v_{exp}$ ($cm^{-1}$) | $v_{aquo}$ ($cm^{-1}$) | $f_{exp}$ ($\times10^{-6}$) | $f_{cal}$ ($\times10^{-6}$) |
|---|---|---|---|---|
| $^6H_{9/2}$ | 7686 | 7700 | 1.44 | 0.54 |
| $^6F_{11/2}$ | 7974 | 7700 | 2.70 | 4.03 |
| $^6F_{9/2}$ | 9199 | 9100 | 1.34 | 3.08 |
| $^6H_{7/2}$ | 9451 | 9100 | 0.66 | 0.14 |
| $^6F_{7/2}$ | 11,350 | 11,000 | 1.75 | 3.02 |
| $^6F_{5/2}$ | 12,642 | 12,400 | 1.10 | 1.51 |
| $^4F_{7/2}$ | 25,680 | 25,800 | 0.26 | 0.26 |
| $^4I_{13/2}$ | 26,125 | 25,800 | 0.67 | 0.61 |
| $^6P_{5/2}$ | 27,700 | 27,400 | 1.06 | 0.67 |
| $^6P_{7/2}$ | 28,830 | 28,550 | 2.83 | 2.38 |
| $^6P_{3/2}$ | 31,055 | 30,892 | 1.01 | 1.18 |
| $^4L_{19/2}$ | 32,154 | 32,187 | 0.45 | 0.17 |
| | $\bar{\beta} = 1.014$, $\delta = -1.38$ | | rms = $0.94 \times 10^{-6}$ | |

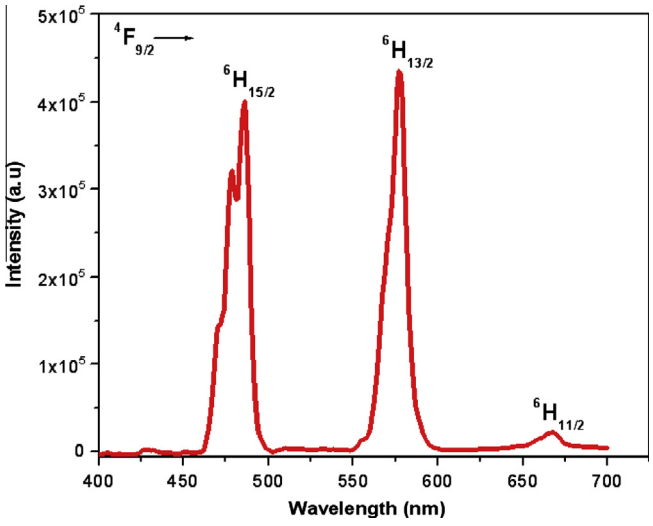


**Fig. 2.** The emission spectrum of $K_2GdF_5$:$Dy^{3+}$crystal.

$\|U^6\|^2 = 0.0303$, because $\|U^2\|^2 = 0$ and $\|U^4\|^2 = 0.0049$ (see Table 5 in Ref. [14]). Therefore the intensity ratio of yellow emission–blue emission (Y/B) should increase when the $\Omega_2$ value increase [14,22], consequently it is influenced by site asymmetries and electro-negativities of the ligand ions [23,24].

The yellow–blue (Y/B) intensity ratio is especially interested for lighting technology because the line linking the yellow and blue wavelengths in the CIE 1931 chromaticity diagram usually passes through the white light region. Therefore, the chromaticity coordinates of the phosphors containing $Dy^{3+}$ can be adjusted to the white light zone by adjusting to a suitable Y/B ratio [25,26]. In our experiment, under 365 nm UV excitation, yellow and blue emission bands are observed in the emission spectrum, which presents the chromaticity coordinates ($x = 0.275$, $y = 0.292$) and locates in the white light region of the CIE 1931 chromaticity diagram.

It is interesting to note that, in our sample, the calculated Y/B intensity ratio is roughly 1.9 times larger than the corresponding obtained our experimental values (Table 4). This large discrepancy is observed also in many other fluorides compounds [22]. It is evident for example that, for the materials with low $\Omega_2$ parameter, the Judd–Ofelt approach could quantatively overestimate the relative intensity of the yellow emission with respect to that of the blue one [22].

On the basis of 30 energy levels recorded in absorption, emission and excitation spectra some considerations have been used for the experimental energy level assignment: first of all, these spectra are characterized by a strong inhomogeneous broadening of the disordered structure therefore some discrepancy was observed between the absorption and emission lines. Then, the rare earth ion being located in a low symmetry site $C_{2v}$, some levels should be split into many sub-levels which have many different barycenters. Finally, according to the energy diagram of $Dy^{3+}$ ions [20], the transitions are assigned. The wavelengths corresponding to the transitions are listed in Table 3.

### 4.2. Energy transfer between $Gd^{3+}$ and $Dy^{3+}$ions

The UV excitation spectra of the $Dy^{3+}$ emission at the wavelengths 575 nm and 485 nm of the $K_2GdF_5$:$Dy^{3+}$ crystals are shown in Fig. 3. Two narrow lines peaking at 254 nm and 273 nm are observed in the UV-side, which correspond to the transitions from the ground state $^8S_{7/2}$ of $Gd^{3+}$ ion to its excited states $^6D_J$ ($J = 7/2, 9/2$) and $^6I_{11/2}$ respectively [27]. These lines are not observed in the excitation and absorption spectra of the $Dy^{3+}$-doped samples without $Gd^{3+}$ component [28,29]. This implies that energy transfer from $Gd^{3+}$ to $Dy^{3+}$ ions occurred in this crystal. Consequently, the luminescence of $Dy^{3+}$ ions in $K_2GdF_5$ could be strongly excited by the additional light with 254 nm and 273 nm wavelengths.

### 4.3. Bonding characteristic, J–O parameters

The bonding parameter ($\delta$) is defined as $\delta = [(1 - \bar{\beta})/\bar{\beta}] \times 100$ [15,16], where $\bar{\beta} = (\sum \beta)/n$ and $\beta$ (nephelauxetic ratio) = $v_c/v_a$, $v_c$ and $v_a$ are energies of the corresponding transitions in the complex and aqua-ion [11], respectively, and $n$ is refers to the number of levels that are used to compute $\bar{\beta}$ values. The bonding parameter depends on the environmental field; $\delta$ can be received the positive or negative value indicating covalent or ionic bonding. In our sample, the values of $\bar{\beta}$ and $\delta$ bonding parameter are 1.014, −1.38, respectively. Thus, in this case the bonding of $Dy^{3+}$ ions with the local host is ionic bonding.

The experimental ($f_{exp}$) oscillator strengthss of twelve absorption bands were determined using Eq. (1) and the absorption spectrum of the $K_2GdF_5$:$Dy^{3+}$ crystal, as shown in table 1. All these absorption bands have been analyzed using JO theory and were least squared fitted to yield the best fit values for the JO parameters $\Omega_2$, $\Omega_4$ and $\Omega_6$. The reduced matrix elements were taken from Jayasankar et al. [14]. The accuracy of the fit is given by the rms deviation between the experimental ($f_{exp}$) and calculated ($f_{cal}$) oscillator strengths. In our case, the best-fitted JO parameters are $\Omega_2 = 2.51 \times 10^{-20}\,cm^2$, $\Omega_4 = 0.94 \times 10^{-20}\,cm^2$ and $\Omega_6 = 2.12 \times 10^{-20}\,cm^2$ with the rms deviation of $0.94 \times 10^{-6}$. In comparison to other host lattices, as presented in Table 2, the $\Omega_2$ value of our crystal is smaller than that of the different hosts. According to the JO theory, the $\Omega_\lambda$ parameters are determined by formula

**Table 2**
The JO parameters for $Dy^{3+}$ doped various hosts.

| Host matrix | $\Omega_2$ ($\times10^{-20}$ cm$^2$) | $\Omega_4$ ($\times10^{-20}$ cm$^2$) | $\Omega_6$ ($\times10^{-20}$ cm$^2$) | Refs. |
|---|---|---|---|---|
| $K_2GdF_5$:$Dy^{3+}$ | 2.51 | 0.94 | 2.12 | Present |
| $K_2SO_4$–$ZnSO_4$–$B_2O_3$ | 52.44 | 5.80 | 6.81 | [14] |
| $ZnSO_4$–$B_2O_3$ | 34.48 | 3.06 | 9.12 | [14] |
| $Li_2SO_4$–$ZnSO_4$–$B_2O_3$ | 21.01 | 8.13 | 7.54 | [14] |
| $Na_2SO_4$–$ZnSO_4$–$B_2O_3$ | 16.82 | 9.45 | 6.50 | [14] |
| $GeO_2$–$B_2O_3$–$Z_nO$–$LaF_3$ | 15.73 | 2.46 | 5.49 | [17] |
| $PbO_5$–$K_2O$–$BaO$–$AlO_3$–$AlF_3$ | 12.3 | 2.67 | 2.30 | [15] |
| $SiO_2$–$Al_2O_3$–$LiF$–$GdF_3$ | 4.53 | 0.66 | 2.40 | [17] |
| $PbO$–$PbF_2$ | 2.13 | 2.10 | 1.0 | [16] |
| $KY_3F_{10}$ | 1.55 | 1.81 | 1.63 | [22] |
| $LiLuF_{10}$ | 2.04 | 0.91 | 1.09 | [22] |
| $BaY_2F_8$ | 1.52 | 2.33 | 3.67 | [33] |
| $LiYF_4$ | 2.01 | 1.34 | 2.39 | [35] |

**Table 3**
Transition energies ($v$), radiative transition probabilities ($S_{ed}$, $S_{md}$, $A$ and $A_T$), radiative lifetime ($\iota_R$) and branching ratios ($\beta_R$) for excited levels.

| $SLJ$ | $S'L'J'$ | $v$ (cm$^{-1}$) | $S_{ed}$ ($\times10^{-40}$ cm$^2$) | $S_{md}$ ($\times10^{-40}$ cm$^2$) | $A$ (s$^{-1}$) | $\beta_R$ (%) |
|---|---|---|---|---|---|---|
| $^4F_{9/2}$ | $^6F_{1/2}$ | 7291 | 0.01 | 0 | 0.03 | 0 |
| | $^6F_{3/2}$ | 7902 | 0.01 | 0 | 0.08 | 0.01 |
| | $^6F_{5/2}$ | 8556 | 0.41 | 0 | 2.85 | 0.29 |
| | $^6F_{7/2}$ | 9946 | 0.26 | 0.40 | 3.39 | 0.48 |
| | $^6H_{5/2}$ | 10,900 | 0.14 | 0 | 1.91 | 0.57 |
| | $^6H_{7/2}$ | 11,963 | 0.58 | 0.18 | 11.1 | 1.84 |
| | $^6F_{9/2}$ | 12,066 | 0.19 | 0.16 | 3.98 | 0.67 |
| | $^6F_{11/2}$ | 13,258 | 0.41 | 0.02 | 10.40 | 1.75 |
| | $^6H_{9/2}$ | 13,398 | 0.35 | 1.65 | 14.20 | 2.39 |
| | $^6H_{11/2}$ | 15,209 | 0.77 | 0.31 | 30.80 | 5.17 |
| | $^6H_{13/2}$ | 17,628 | 6.13 | 0 | 358.00 | 60.00 |
| | $^6H_{15/2}$ | 21,182 | 1.59 | 0 | 160.25 | 26.80 |
| | | | $A_T(^4F_{9/2})$ = 596 s$^{-1}$; $\iota_R(^4F_{9/2})$ = 1.68 ms | | | |
| $^6F_{5/2}$ | $^6F_{7/2}$ | 1390 | 3.05 | 20.60 | 0.29 | 0.03 |
| | $^6H_{5/2}$ | 2344 | 7.98 | 0.01 | 1.83 | 0.16 |
| | $^6H_{7/2}$ | 3407 | 33.20 | 0 | 21.30 | 2.15 |
| | $^6F_{9/2}$ | 3510 | 2.72 | 0 | 1.88 | 0.19 |
| | $^6F_{11/2}$ | 4702 | 5.64 | 0 | 10.50 | 1.08 |
| | $^6H_{9/2}$ | 4842 | 23.50 | 0 | 44.60 | 4.59 |
| | $^6H_{11/2}$ | 6653 | 11.70 | 0 | 60.40 | 6.22 |
| | $^6H_{13/2}$ | 9072 | 18.60 | 0 | 238.00 | 24.50 |
| | $^6H_{15/2}$ | 12,626 | 17.10 | 0 | 592.00 | 61.00 |
| | | | $A_T(^4F_{5/2})$ = 971 s$^{-1}$; $\iota_R(^4F_{5/2})$ = 1.03 ms | | | |
| $^6F_{11/2}$ | $^6H_{9/2}$ | 29 | 27.20 | 1.19 | 0 | 0 |
| | $^6H_{11/2}$ | 1908 | 45.40 | 0.59 | 2.80 | 0.79 |
| | $^6H_{13/2}$ | 4259 | 62.10 | 1.28 | 42.70 | 11.70 |
| | $^6H_{15/2}$ | 7779 | 81.60 | 0 | 341.00 | 87.5 |
| | | | $A_T(^4F_{11/2})$ = 387 s$^{-1}$; $\iota_R(^4F_{11/2})$ = 2.59 ms | | | |
| $^6H_{9/2}$ | $^6H_{11/2}$ | 1879 | 24.20 | 36.00 | 2.03 | 2.52 |
| | $^6H_{13/2}$ | 4230 | 25.10 | 0 | 20.20 | 27.20 |
| | $^6H_{15/2}$ | 7750 | 10.20 | 0 | 50.6 | 70.20 |
| | | | $A_T(^4H_{9/2})$ = 72.9 s$^{-1}$; $\iota_R(^4H_{9/2})$ = 13.7 ms | | | |
| $^6H_{11/2}$ | $^6H_{13/2}$ | 2351 | 23.80 | 32.80 | 3.22 | 4.40 |
| | $^6H_{15/2}$ | 5871 | 38.20 | 0 | 68.70 | 95.6 |
| | | | $A_T(^4H_{11/2})$=71.9 s$^{-1}$; $\iota_R(^4H_{11/2})$ = 13.9 ms | | | |
| $^6H_{13/2}$ | $^6H_{15/2}$ | 3520 | 56.70 | 22.30 | 23.00 | 100 |
| | | | $A_T(^4H_{13/2})$ = 23 s$^{-1}$; $\iota_R(^4H_{13/2})$ = 43.4 ms | | | |

**Table 4**
Emission peak positions ($\lambda_p$), effective line width ($\Delta\lambda_{eff}$), radiative transition probabilities ($A$), branching ratios ($\beta_{exp}$), stimulated emission cross-section $\sigma(\lambda_P)$ and integrated emission cross-section ($\Sigma_{if}$) for $^4F_{9/2} \rightarrow {}^6H_J$ transitions of $Dy^{3+}$:$K_2GdF_5$ crystal.

| $^4F_{9/2}\rightarrow$ | $\lambda_p$ (nm) | $\Delta\lambda_{eff}$ (nm) | $A$ (s$^{-1}$) | $\sigma(\lambda_p)$ ($\times10^{-22}$ cm$^2$) | $\Sigma_{if}$ ($\times10^{-18}$ cm) | $\beta_R$ (%) | |
|---|---|---|---|---|---|---|---|
| | | | | | | Exp | Cal |
| $^6H_{11/2}$ | 667 | 16.94 | 30.80 | 1.90 | 0.07 | 2.34 | 5.17 |
| $^6H_{13/2}$ | 577 | 15.84 | 358.00 | 13.6 | 1.04 | 53.23 | 60.00 |
| $^6H_{15/2}$ | 485 | 14.61 | 160.00 | 3.60 | 0.23 | 44.43 | 26.80 |

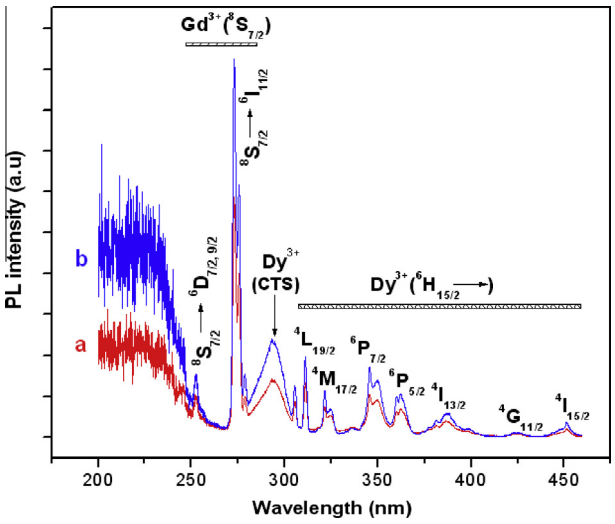


**Fig. 3.** The excitation spectra of the $Dy^{3+}$:$K_2GdF_5$ crystal at the emission wavelengths 575 nm (a) and 485 nm (b).

$$\Omega_\lambda = (2\lambda+1)\sum_{p,s}|A_{sp}|^2\Xi^2_{(s,\lambda)}(2s+1)^{-1} \quad (4)$$

where $A_{sp}$ are the sets of odd-parity terms of the crystal field and where $\Xi_{(s,\lambda)}$ represents a complicated sum over all excited configurations of terms, containing factor like

$$\frac{\langle 4f|r|nl\rangle\langle nl|r^s|4f\rangle}{\Delta E(nl)}$$

where $\Delta E(nl)$ are the energy difference and $\langle 4f|r^k|nl\rangle$ are the radial integrals between the $4f^N$ and the excited $4f^{N-1}nl^1$ configurations. The most important contribution to the mixing of wavefunctions with odd-parity is the 5d orbital [30].

It is worth to point out that, the contribution of the radial intergrals to $\Omega_\lambda$ strongly increases with increasing $\lambda$ value, since larger $\lambda$ takes larger $s$ ($s = \lambda \pm 1$) [24,27]. Therefore, the $\Omega_6$ is more influenced by changes in the radial integrals $\langle 4f|r^s|5d\rangle$ whereas the $\Omega_2$ is more sensitive to the local environment of the RE ions and is often related with the asymmetry of the local crystal field and by changes of the energy difference between the $4f^N$ and $4f^{N-1}5d^1$ configurations [15,16,23,27].

It is well-known, the $K_2LnF_5$ phases with Ln = Y, Nd...Lu crystallize in the orthorhombic system [31]. The $LnF_7$ polyhedra form chains parallel to *c*-axis of structure. The small values of $\Omega_2$ in this system indicate that the $Dy^{3+}$ ions occupy ionic sites with small distortions from orthorhombic system. In our case, the $F^{-1}$ ions have high electronegative (≈4, in Pauling scale), therefore the $Dy^{3+}$–$F^{-1}$ bond has the small covalence ($\delta < 0$), so the $\Delta E = E(4f^N) - E(4f^{N-1}5d)$ is large. This also is a main reason to explain for the reduction of the $\Omega_2$ values in the fluoride compounds.

### 4.4. Fluorescence properties

The radiative properties such as the electric ($S_{ed}$) and magnetic ($S_{md}$) dipole line strengths, the radiative transition rates ($A_R$), radiative lifetime ($\tau_R$), branching ratios ($\beta_R$) were calculated by using JO parameters for six excited levels. The results were showed in Table 3.

From the emission spectrum of $K_2GdF_5$:$Dy^{3+}$, the emission peak positions ($\lambda_p$), effective line width ($\Delta\lambda_{eff}$), calculated radiative transition probabilities ($A$), measured branching ratios ($\beta_{exp}$), stimulated emission cross-section $\sigma(\lambda_P)$ and integrated emission cross-section ($\Sigma_{if}$) were calculated for $^4F_{9/2} \rightarrow {}^6H_J$ ($J$ = 15/2, 13/2, 11/2) transitions. The results were displayed in table 4.

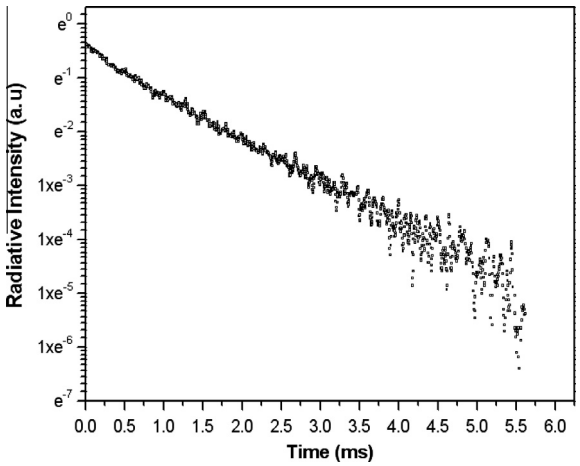


**Fig. 4.** Decay profile of the room temperature emission from the $^4F_{9/2}$ level of 10% $Dy^{3+}$-doped $K_2GdF_5$ crystal.

Murthy et al. [32] reported that the luminescence branching ratio characterizes the possibility of attaining stimulated emission from any specific transition, so it is a critical parameter to the laser designer. In this work, the predicted branching ratio of $^4F_{9/2} \rightarrow {}^6H_{13/2}$ transition get a maximum value and be 60.0% where as the measured ratio is 53.2%. Thus there is a good agreement between experimental and calculated branching ratios.

The experimental luminescence decay is presented in Fig. 4. The measured and calculated lifetime of $^4F_{9/2}$ level is 1.04 ms and 1.68 ms, respectively. The comparison with other fluoride compounds indicates that, this difference is not so large as that was reported by Bigotta et al. [22] but is similar with the values published by Parisi et al. [33]. In any case, this discrepancy between the measured and calculated lifetime indicates that the non-radiative processes are not negligible and they reduce the quantum efficiency of the luminescence progress. The luminescence quantum efficiency of the fluorescent level is defined as the ratio of the measured lifetime to the calculated lifetime by JO theory, $\eta = \tau_{mes}/\tau_R$. In this case, the luminescence quantum efficiency is 61.9%. This relatively high value together with the slightly non-exponential decay profile in Fig. 4 indicates that the non-radiative processes are not too strong even at high-doping level of this material. This non-exponential character of the decay curve could be originated from the concentration quenching. Because of the low phonon energy of the fluoride compounds [30] and the large energy separation between the $^4F_{9/2}$ and $^6H_{13/2}$ manifolds (about 7300 $cm^{-1}$) the multiphonon relaxation between these manifolds is negligible. Therefore the main origin for the non-radiative processes may be attributed to the energy transfer between the activators. The similar behavior is observed also for $Dy^{3+}$ in other host [34].

Besides, the integrated emission cross section, $\Sigma_{if}$, the stimulated emission cross-section, $\sigma(\lambda_P)$, are important parameters that affects the potential laser performance and its value signifies rate of energy extraction from the lasing material [6,15–17]. When the integrated emission cross section is greater than $10^{-18}$ cm, laser emission is probable if the upper state displays a proper lifetime, that is, if it has high quantum efficiency. In our case, with the $^4F_{9/2} \rightarrow {}^6H_{13/2}$ transition, the integrated emission cross-section is $1.04 \times 10^{-18}$ cm.

It is found that $^4F_{9/2} \rightarrow {}^6H_{13/2}$ transition exhibits maximum $\sigma(\lambda_P)$ ($13.6 \times 10^{-22}$ $cm^2$). The large values of branching ratio, integrated emission cross section, luminescence quantum efficiency and stimulated emission cross section suggest that the $^4F_{9/2} \rightarrow {}^6H_{13/2}$ transition can give rise to lasing action.

## 5. Conclusions

In summary, this work investigates a detailed picture of the spectral characteristics of $Dy^{3+}$ ions in $K_2GdF_5$ crystal. The experimental and calculated oscillator strengths of absorption transitions of $K_2GdF_5$:$Dy^{3+}$ were investigated. The intensity parameters ($\Omega_\lambda$) and predicted radiative lifetime ($\iota_R$), branching ratios ($\beta_R$) were determined using JO theory The bonding of $Dy^{3+}$ ions with the $K_2GdF_5$ local host is ionic bonding and the coordination structure surrounding the RE ion has high symmetry were confirmed by the negative value of bonding parameter $\delta$ and the small value of intensity parameter $\Omega_2$. The energy transfer effect was appeared between $Gd^{3+}$ and $Dy^{3+}$ in $K_2GdF_5$ host. This material is a promising material in the efficient laser, white fluorescence lamp.

## Acknowledgments

The authors gratefully acknowledge support for this research from Vietnam's National Foundation for Science and Technology Development (NAFOSTED) with project code 103.06-2011.58 and from Basic Science Research Program (NRF2011-0010155) and Priority Research Centers Program through the National Research Foundation of Korea fund (NRF 2010-0029634).

## References

[1] A.J. Kenyon, Prog. Quant. Electron. 26 (2002) 225–284.
[2] J. Fiebrandt, E. Lindner, S. Brückner, M. Becker, A. Schwuchow, M. Rothhardt, H. Bartelt, Opt. Commun. 285 (2012) 5157–5162.
[3] M. Joseph, P. Manoravi, N. Sivakumar, R. Balasubramanian, Int. J. Mass Spectrom. 253 (2006) 98–103.
[4] S. Dardona, A. Konjhodzic, D. Chhabria, O. Salihoglu, Z. Hasan, J. Lumin. 107 (2004) 182–186.
[5] V. Venkatramu, P. Babu, C.K. Jayasankar, T. Tröster, W. Sievers, G. Wortmann, Opt. Mater. 29 (2007) 1429–1439.
[6] D. Wang, Y. Guo, Q. Wang, Z. Chang, J. Liu, J. Luo, J. Alloys Comp. 474 (2009) 23–25.
[7] N. Kristianpoller, D. Weiss, N. Khaidukov, V. Makhov, R. Chen, Radiat. Meas. 43 (2008) 245–248.
[8] H.K. Hanh, N.M. Khaidukov, V.N. Makhov, V.X. Quang, N.T. Thanh, V.P. Tuyen, Nucl. Instrum. Methods Phys. Res., Sect. B 268 (2010) 3344–3350.
[9] P. Van Do, V.P. Tuyen, V.X. Quang, N.T. Thanh, V.T.T. Ha, N.M. Khaidukov, Y.-I. Lee, B.T. Huy, J. Alloys Comp. 520 (2012) 262–265.
[10] J. Marcazzó, E. Cruz-Zaragoza, V. Xuan Quang, N.M. Khaidukov, M. Santiago, J. Lumin. 131 (2011) 2711–2715.
[11] J. Marcazzo, M. Santiago, E. Caselli, N. Nariyama, N.M. Khaidukov, Opt. Mater. 26 (2004) 65–70.
[12] D. Wang, Y. Min, S. Xia, V.N. Makhov, N.M. Khaidukov, J.C. Krupa, J. Alloys Comp. 361 (2003) 294–298.
[13] K.H. Jang, E.S. Kim, L. Shi, N.M. Khaidukov, H.J. Seo, Opt. Mater. 31 (2009) 1819–1821.
[14] C.K. Jayasankar, E. Rukmini, Physica B 240 (1997) 273–288.
[15] R. Praveena, R. Vijaya, C.K. Jayasankar, Spectrochim. Acta Part A Mol. Biomol. Spectrosc. 70 (2008) 577–586.
[16] P. Nachimuthu, R. Jagannathan, V. Nirmal Kumar, D. Narayana Rao, J. Non-Cryst. Solids 217 (1997) 215–223.
[17] G. Lakshminarayana, J. Qiu, Physica B 404 (2009) 1169–1180.
[18] B.T. Huy, Min-Ho Seo, Jae-Min Lim, Yong-Ill Lee, N.T. Thanh, V.X. Quang, T.T. Hoai, N.A. Hong, J. Korean Phys. Soc 59 (2011) 3300–3307.
[19] B.R. Judd, Phys. Rev. 127 (1962) 750–761.
[20] G.S. Ofelt, J. Chem. Phys. 37 (1962) 511–520.
[21] W.T. Carnall, P.R. Fields, K. Rajnak, J. Chem. Phys. 49 (1968) 4424–4442.
[22] S. Bigotta, M. Tonelli, E. Cavalli, A. Belletti, J. Lumin. 130 (2010) 13–17.
[23] R. Peacock, The intensities of lanthanide f ↔ f transitions, in: Rare Earths, Springer, Berlin Heidelberg, 1975, pp. 83–122.
[24] H. Ebendorff-Heidepriem, D. Ehrt, J. Non-Cryst. Solids 248 (1999) 247–252.
[25] Q. Su, H. Liang, C. Li, H. He, Y. Lu, J. Li, Y. Tao, J. Lumin. 122–123 (2007) 927–930.
[26] Q. Su, Z. Pei, L. Chi, H. Zhang, Z. Zhang, F. Zou, J. Alloys Comp. 192 (1993) 25–27.
[27] K. Binnemans, C. Görller-Walrand, J.L. Adam, Chem. Phys. Lett. 280 (1997) 333–338.
[28] G. Lakshminarayana, H. Yang, J. Qiu, J. Solid State Chem. 182 (2009) 669–676.
[29] P. Babu, K.H. Jang, E.S. Kim, L. Shi, R. Vijaya, V. Lavín, C.K. Jayasankar, H.J. Seo, J. Non-Cryst. Solids 356 (2010) 236–243.
[30] R. Reisfeld, Spectra and energy transfer of rare earths in inorganic glasses, in: Rare Earths, Springer, Berlin Heidelberg, 1973, pp. 53–98.
[31] H. Kharbache, R. Mahiou, P. Boutinaud, D. Boyer, D. Zakaria, P. Deren, Opt. Mater. 31 (2009) 558–561.
[32] D.V.R. Murthy, T. Sasikala, B.C. Jamalaiah, A.M. Babu, J.S. Kumar, M. Jayasimhadri, L. Rama Moorthy, Opt. Commun. 284 (2011) 603–607.
[33] P. Daniela, T. Alessandra, T. Mauro, C. Enrico, B. Enrico, B. Alessandro, J. Phys.: Condens. Matter 17 (2005) 2783.
[34] Y. Wei, C. Tu, H. Wang, F. Yang, G. Jia, Z. You, X. Lu, J. Li, Z. Zhu, Y. Wang, J. Alloys Comp. 438 (2007) 310–316.
[35] M.G. Brik, T. Ishii, A.M. Tkachuk, S.E. Ivanova, I.K. Razumova, J. Alloys Comp. 374 (2004) 63–68.